LANGMUIR

pubs.acs.org/Langmuir Article

Elucidating How Different Amphipathic Stabilizers Affect BSA Protein Conformational Properties and Adsorption Behavior

Gamaliel Junren Ma, Abdul Rahim Ferhan, Joshua A. Jackman,* and Nam-Joon Cho*

Cite This: *Langmuir* 2020, 36, 10606−10614 Read Online

ACCESS | Metrics & More | Article Recommendations | Supporting Information

ABSTRACT: Natural proteins such as bovine serum albumin (BSA) are readily extracted from biological fluids and widely used in various applications such as drug delivery and surface coatings. It is standard practice to dope BSA proteins with an amphipathic stabilizer, most commonly fatty acids, during purification steps to maintain BSA conformational properties. There have been extensive studies investigating how fatty acids and related amphiphiles affect solution-phase BSA conformational properties, while it is far less understood how amphipathic stabilizers might influence noncovalent BSA adsorption onto solid supports, which is practically relevant to form surface coatings. Herein, we systematically investigated the binding interactions between BSA proteins and different molar ratios of caprylic acid (CA), monocaprylin (MC), and methyl caprylate (ME) amphiphiles—all of which have 8-carbon-long, saturated hydrocarbon chains with distinct headgroups—and resulting effects on BSA adsorption behavior on silica surfaces. Our findings revealed that anionic CA had the greatest binding affinity to BSA, which translated into greater solution-phase conformational stability and reduced adsorption-related conformational changes along with relatively low packing densities in fabricated BSA adlayers. On the other hand, nonionic MC had moderate binding affinity to BSA and could stabilize BSA conformational properties in the solution and adsorbed states while also enabling BSA adlayers to form with higher packing densities. We discuss physicochemical factors that contribute to these performance differences, and our findings demonstrate how rational selection of amphiphile type and amount can enable control over BSA adlayer properties, which could lead to improved BSA protein-based surface coatings.

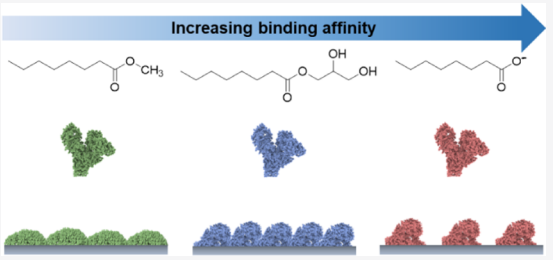

INTRODUCTION

The phenomenon of noncovalent protein adsorption at solid−liquid interfaces is closely linked with a wide range of medical and biotechnology applications, including implantable medical devices, biosensors, and drug-delivery systems.[1−5] Mechanistically, the protein adsorption process is governed by a combination of protein−surface interactions and lateral protein−protein interactions between adsorbed proteins.[6−8] Importantly, both protein−surface and protein−protein interactions can be modulated depending on key molecular properties of the adsorbing protein, which opens the door to controlling protein adsorption processes based on molecular design strategies in line with the nanoarchitectonics concept.[9,10]

Toward this objective, a popular strategy involves tuning the thermodynamic stability of the folded protein structure in bulk solution—termed conformational stability—as a means to modulate protein adsorption behavior. For example, Karlsson et al. experimentally showed that certain synthetic mutants of the carbonic anhydrase II protein, which were engineered (via amino acid substitution) to have lower conformational stability, underwent more extensive surface-induced denaturation and exhibited greater adsorption irreversibility on various solid supports.[11] The conformational stability of natural proteins can also be modulated by adjusting environmental conditions, such as temperature, solution pH, and solvent conditions, which in turn affect protein adsorption behavior. This latter approach has been applied to bovine serum albumin (BSA), which is a widely studied protein that is isolated from bovine plasma and commonly used as a reagent for blocking and surface passivation applications.[12−17] For example, Park et al. reported that heat pretreatment converts BSA protein monomers into oligomers, which adsorb onto solid surfaces to a greater extent than monomers at room temperature due to distinct conformational properties and consequently exhibit superior surface passivation properties.[13] It is also important to consider how the interactions of BSA with other types of molecules affect protein structure and function.

As part of processing methods to isolate BSA proteins from crude protein mixtures, fatty acids, most often caprylic acid (CA), are widely used as dopants to endow BSA proteins with greater stability during high-temperature extraction steps. Fatty

Received: July 12, 2020
Revised: August 4, 2020
Published: August 11, 2020

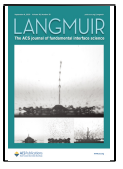

https://dx.doi.org/10.1021/acs.langmuir.0c02048
Langmuir 2020, 36, 10606−10614

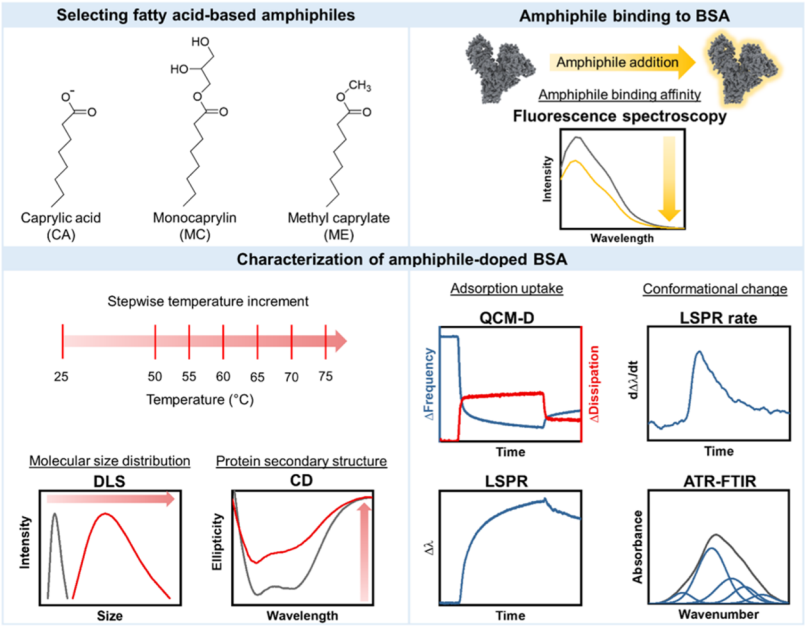

Figure 1. Overview of experimental strategy. The binding interactions of BSA with different amphipathic molecules, namely, CA, MC, and ME, were quantitively characterized by fluorescence spectroscopy along with dynamic light scattering (DLS) and circular dichroism (CD) spectroscopy measurements to evaluate solution-phase conformational stability. Quartz crystal microbalance-dissipation (QCM-D), localized surface plasmon resonance (LSPR), and attenuated total reflection-Fourier transform infrared (ATR-FTIR) spectroscopy experiments were conducted to determine how binding interactions with the tested amphipathic molecules affected BSA protein adsorption behavior in terms of adsorption uptake and kinetics along with related conformational changes.

acids and related amphipathic molecules with hydrophilic headgroups and hydrophobic chains are known to bind to BSA proteins through hydrophobic, electrostatic, and hydrogen-bonding interactions.[18−20] There have been extensive studies investigating how factors such as amphiphile chain length[21−23] and headgroup properties[24−28] affect the binding of amphipathic molecules to BSA proteins along with the extent of solution-phase conformational stability in response to chemical and thermal denaturants.[29−31] On the other hand, it was only recently observed that fatty acid doping also significantly affects protein adsorption and resulting surface passivation performance.[32] In particular, fatty acid-doped BSA proteins exhibit less adsorption uptake and adsorption-related denaturation on silica surfaces as well as reduced surface passivation performance, compared to fatty acid-free BSA proteins. These effects are related to (1) greater conformational stability and (2) more repulsive protein−protein interactions of fatty acid-doped BSA molecules, the latter of which originates from the anionic character of bound fatty acids and results in a lower surface coverage of adsorbed proteins. At the same time, there remains an outstanding need to more broadly understand how different molecular features of amphipathic molecules, including fatty acids and related compounds, affect BSA adsorption behavior.

Herein, we investigated how the binding interactions of CA fatty acid and its monoglyceride and methyl ester derivatives termed monocaprylin (MC) and methyl caprylate (ME), respectively, with BSA proteins affect BSA adsorption behavior on silica surfaces by utilizing a combination of biophysical and surface-sensitive measurement techniques. The overall experimental strategy is presented in Figure 1. All three compounds have an 8-carbon-long saturated hydrocarbon chain along with distinct headgroup properties. The anionic CA headgroup consists of a carboxylic acid functional group, while the nonionic MC headgroup is formed from the conjugation of a hydrophilic glycerol molecule to CA and the nonionic ME headgroup is formed by the addition of a hydrophobic methyl group to the carboxylic acid of CA. Particular attention was focused on scrutinizing how CA, MC, and ME affect solution-phase BSA conformational stability in the broader context of tracking protein adsorption uptake and kinetics along with related conformational changes in the adsorbed state.

MATERIALS AND METHODS

Reagents. Fatty acid-free BSA (A7030, lot no. SLBT4132), octanoic acid (caprylic acid, C2875), 1-monocapryloyl-*rac*-glycerol (monocaprylin, M2265), methyl octanoate (methyl caprylate, 260673), sodium dodecyl sulfate (SDS, L4390), sodium chloride (NaCl, 746398), and sodium hydroxide (S5881) were purchased from Sigma-Aldrich. Tris(hydroxymethyl)aminomethane (Tris, 0497) was purchased from Amresco. Ethanol (95%) was purchased from Aik Moh (Singapore), and hydrochloric acid (HCl, 100317) was purchased from Merck.

Sample Preparation. An aqueous buffer solution of 10 mM Tris, 150 mM NaCl, and pH 7.5 was prepared with Milli-Q-treated water (resistivity of >18.2 MΩ·cm at 25 °C) and filtered through a 0.2 μm polyethersulfone (PES) membrane filter (Thermo Fisher Scientific, 595-4520). BSA solutions were prepared by dissolving lyophilized BSA powder in the buffer solution and then filtering the BSA suspension through a syringe filter with 0.2 μm diameter pores (PN-4612; Pall Corporation). The molar concentrations of the BSA protein in aqueous buffer solution was determined by UV light absorbance measurements at 280 nm, and the molar extinction coefficient value of BSA was taken to be 43 824 M^{-1} cm^{-1}. To prepare CA-doped BSA, CA was dissolved in protein-free Tris buffer, followed by NaOH titration, to make a 50 mM CA solution at pH 7.5. The CA solution was then added to appropriate amounts of BSA solution to yield CA-doped BSA samples with a CA/BSA molar ratio of 10:1 (CA 10) or 100:1 (CA 100). MC and ME solutions were made by dissolving appropriate amounts in equivalent buffer solution to make 20 mM MC or ME solutions, followed by heating to 70 °C for 30 min

https://dx.doi.org/10.1021/acs.langmuir.0c02048
Langmuir 2020, 36, 10606−10614

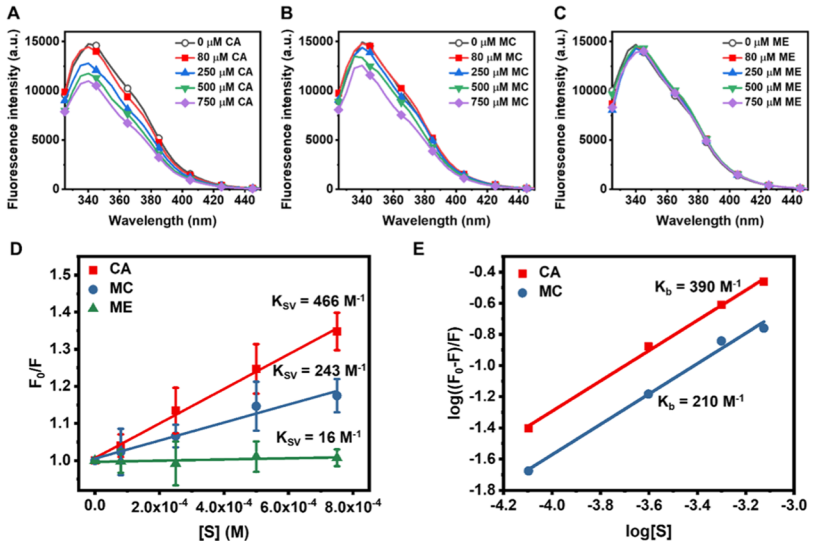

Figure 2. Evaluation of CA, MC, and ME binding interactions with BSA proteins. (A–C) Intrinsic fluorescence emission spectra of 10 μM BSA in the absence and presence of (A) CA, (B) MC, and (C) ME amphiphiles. (D) Stern–Volmer plots corresponding to the data in (A)–(C). Data are presented as mean ± standard deviation (sd). Linear fits and corresponding K_{SV} values of CA, MC, and ME binding to BSA are presented for each data set. (E) Plot of $\log((F_0 - F)/F)$ versus log[S]. Linear fits and the corresponding K_b values of CA and MC binding to BSA are presented for each data set.

to aid dissolution. The samples were then cooled down to room temperature before adding appropriate amounts of BSA solution to yield MC- or ME-doped BSA samples with MC/BSA and ME/BSA molar ratios of 10:1 (MC 10 and ME 10) and 100:1 (MC 100 and ME 100).

Fluorescence Spectroscopy. The intrinsic fluorescence of BSA protein samples was characterized by fluorescence spectroscopy measurements using a Tecan Spark plate reader (Tecan, Switzerland) with the temperature set to 25 °C, an excitation wavelength of 280 nm, and the emission spectra recorded from 325 to 450 nm. For each sample, the BSA concentration was fixed at 10 μM, while CA, MC, and ME concentrations were varied. All spectra of the BSA samples were recorded in triplicate and subtracted by the background spectra of equivalent test compound concentrations without BSA protein to remove any possible contribution from the CA, MC, or ME background signal alone. The emission maxima for all BSA samples was located at 340 nm, and fluorescence intensity values at this wavelength were used for Stern–Volmer (SV) and binding analyses.

Dynamic Light Scattering. The intensity-weighted size distributions of 150 μM BSA protein samples were determined by the DLS technique using a particle size analyzer (ZetaPALS, Brookhaven Instruments). The BIC Particle Sizing software package (v5.27; Brookhaven Instruments) was used for data collection and analysis. Measurements were first recorded at 25 °C, followed by increasing the temperature from 50 to 75 °C in 5 °C increments, as previously described.[32] Samples were equilibrated for 5 min after each temperature adjustment before measurements were performed. For time-dependent measurements, the samples were equilibrated at 50 °C and then at 55 °C for 10 min each before maintaining a constant temperature of 60 °C and measuring protein size every 10 min for 200 min.

Circular Dichroism Spectroscopy. CD spectroscopy experiments were conducted using an AVIV Model 420 CD spectrometer with the AVIV CDS software package (v3.36 MX) (AVIV Biomedical, Lakewood, NJ). Temperature-dependent measurements were conducted in a similar format to the DLS experiments, as described above. All spectra of the BSA samples were subtracted by background spectra of equivalent conditions, including appropriate CA, MC, or ME concentration, without BSA protein. More details are provided in the Supporting Information.

Quartz Crystal Microbalance-Dissipation. The real-time adsorption of BSA protein samples onto silica surfaces was characterized by QCM-D measurements that were conducted using a QSense E4 instrument (Biolin Scientific AB, Stockholm, Sweden) with silica-coated AT-cut quartz crystal sensor chips with a fundamental frequency of 5 MHz (QSX 303, Biolin Scientific, Sweden). Before every experiment, the sensor chips were sequentially rinsed with 1% (wt/vol) aqueous SDS solution, water, and ethanol and then dried under a gentle stream of nitrogen gas, followed by oxygen plasma treatment (PDC-002, Harrick Plasma) for 3 min. A peristaltic pump was used to inject liquid samples into the measurement chamber at a flow rate of 100 μL/min. A stable baseline signal was first established in Tris buffer solution before 100 μM BSA protein was introduced into the measurement chamber for 30 min, followed by a buffer washing step. The resonance frequency (ΔF) and energy dissipation (ΔD) shifts were recorded in real time at multiple odd overtones, as previously described.[33] All experiments were conducted at 25 °C, and all measurement operations were controlled by the QSoft 401 (v2.5.13.664) (Biolin Scientific) software package. The normalized data at the fifth overtone are reported.

Localized Surface Plasmon Resonance. BSA protein adsorption onto silica-coated gold nanodisk arrays was characterized by ensemble-averaged localized surface plasmon resonance (LSPR) measurements, which were conducted in optical transmission mode using an Insplorion XNano instrument (Insplorion AB, Gothenburg, Sweden), as previously described.[34] The sensor chip preparation and LSPR adsorption experiments were conducted in a similar format to the QCM-D experiments described above. The Insplorer software package (Insplorion AB, Sweden) was used to record the LSPR extinction spectra with a time resolution of 1 Hz, and the centroid (peak) position ($\Delta\lambda$) in the extinction spectrum at each time point was recorded in real time. The rates of change of the $\Delta\lambda$ shifts were also determined by calculating the first derivative with respect to time ($d\Delta\lambda/dt$) (see ref 35) using the OriginPro 2019b software package.

Attenuated Total Reflection-Fourier Transform Infrared Spectroscopy. ATR-FTIR spectroscopy experiments were conducted using a Bruker Vertex 70 FTIR spectrometer with a liquid-nitrogen-cooled mercury cadmium telluride (MCT) photodetector (Bruker, Germany) and equipped with a MIRacle ATR accessory containing a three-reflection ZnSe ATR crystal (PIKE Technologies). The secondary structures of 100 μM BSA proteins in solution and in the adsorbed state were determined by ATR-FTIR spectroscopy experiments, as previously described.[32] More details are provided in the Supporting Information.

https://dx.doi.org/10.1021/acs.langmuir.0c02048
Langmuir 2020, 36, 10606–10614

Statistical Analysis. The tests were conducted using the GraphPad Prism (v8.0.1) software package from GraphPad Software. One-way and two-way analyses of variance (ANOVA) with the appropriate multiple comparisons test were conducted to compute multiplicity-adjusted P values to determine the statistical significance of measurement data as appropriate. All statistical analyses involved two-tailed tests. $P < 0.05$, $P < 0.01$, $P < 0.001$, and $P < 0.0001$ indicate the levels of statistical significance, and NS is "not significant".

RESULTS AND DISCUSSION

Binding Interaction Analysis. We first measured the binding affinities of CA, MC, and ME to solution-phase BSA proteins by steady-state fluorescence spectroscopy (Figure 2 and Table S1). Like how fatty acids can insert into hydrophobic pockets on the BSA protein surface, it is known that monoglycerides[36−38] and fatty acid methyl esters[39,40] can bind similarly to serum albumin proteins in some cases. We evaluated the fluorescence emission spectra corresponding to the intrinsic fluorescence of tryptophan residues in BSA alone and in BSA together with varying amounts of CA, MC, or ME (Figure 2A−C). The excitation wavelength was 280 nm, and the maximum-intensity emission wavelength was 340 nm in all cases. At higher CA and MC concentrations, there was greater quenching, which resulted in a lower maximum intensity at the 340 nm wavelength, while ME had a negligible effect on the intensity value.

To analyze the measurement data, the Stern−Volmer (SV) equation was used[41]

$$\frac{F_0}{F} = 1 + K_{SV}[S] = 1 + k_q\tau_0[S] \quad (1)$$

where F_0 and F are the experimentally determined maximum-intensity values of BSA alone and in the presence of CA, MC, or ME at different concentrations, K_{SV} is the SV quenching constant, [S] is the concentration of amphiphile in the bulk solution, k_q is the bimolecular quenching rate constant, and τ_0 is the average fluorescence lifetime of BSA alone. The SV data are plotted as F_0/F versus [S] for BSA complexes with CA, MC, and ME and shown in Figure 2D. The K_{SV} values were 466, 243, and 16 M^{-1} for CA, MC, and ME binding, respectively, which indicate that CA had the strongest binding interactions with BSA, followed by MC and then ME. Notably, the low K_{SV} value for ME indicates a nearly negligible binding interaction with BSA and thus ME was excluded from further binding analysis.

Taking into account that the value of τ_0 for BSA is 6×10^{-9} s,[27,42] the resulting k_q values for CA and MC are around 7.77×10^{10} and 4.10×10^{10} M^{-1} s^{-1}, respectively, which are indicative of static quenching (see calculation details in the Supporting Information). Next, we determined the effective binding constant (K_b) values for CA and MC according to the following equation[43,44]

$$\log\frac{F_0 - F}{F} = \log K_b + n \log[S] \quad (2)$$

where n is the number of different binding site types, and the corresponding log plot is presented in Figure 2E. The average K_b values were determined to be 390 and 210 M^{-1} for the BSA complexes with CA and MC, respectively, while n was calculated to be 0.97 for both cases. The binding interaction data are summarized in Table S1. The results indicate that anionic CA has the strongest binding affinity with BSA proteins, followed by the polar and nonionic MC. By contrast, the nonionic ME, with the least polar methanol ester headgroup, had the lowest binding affinity to BSA. The calculated n value agrees well with previous works for CA binding[44] and indicates that both amphiphiles bind to a single type of binding site, which consists of hydrophobic pockets on the BSA protein surface. In other words, each amphiphile displayed one mode of binding to BSA. Collectively, the data support that the carboxylic acid headgroup of CA has stronger interactions with BSA, likely through electrostatic interactions and/or hydrogen bonding, while the glycerol ester headgroup of MC forms more extensive hydrogen bonds with BSA compared to the methanol ester headgroup of ME. As such, these findings demonstrate that headgroup polarity strongly influences the binding interaction of amphipathic molecules with BSA proteins even when the different amphiphiles have identical hydrocarbon chains.

Solution-Phase Conformational Stability. We proceeded to compare the effects of CA, MC, and ME doping (10:1 and 100:1 molar ratios of amphiphile/BSA) on the solution-phase conformational stability of BSA by conducting temperature-dependent DLS and CD spectroscopy experiments. A defatted BSA sample without CA, MC, or ME was also tested as a control.

In the DLS measurements, the onset temperature of aggregation was determined by recording the lowest temperature at which a marked increase in the mean hydrodynamic diameter of BSA protein samples occurred. BSA samples with increased conformational stability tend to have a higher onset temperature of aggregation.[32] From 25 to 55 °C, all BSA samples had similar mean hydrodynamic diameters of ∼9 nm (Figures 3A and S1), which is around the expected size of BSA monomers.[12,13,45] At 60 °C, the diameters of defatted BSA and ME samples increased to ∼11 nm, indicating the onset of aggregation. MC 10 and MC 100 samples started aggregating at 65 °C and reached ∼16 and ∼13 nm in diameter, respectively, while CA 10 samples started aggregating at 70 °C and reached ∼15 nm in diameter. Interestingly, at 70 °C, MC 100 aggregated to a larger size than defatted BSA, MC 10, and both ME samples and was about twice the size of these other samples at 75 °C. By contrast, the CA 100:1 sample did not display any evidence of protein aggregation across the tested temperature range. Together, these data indicate that CA doping endows BSA proteins with the highest conformational and/or colloidal stability, followed by MC, whereas ME was essentially ineffective and ME-doped samples behaved almost equivalently to the defatted BSA control.

The data also revealed that CA and MC amphiphiles more effectively decreased the onset temperature of aggregation of BSA proteins with higher bulk concentrations of amphiphile, which would maximize binding site occupancy. Time-dependent size measurements at a constant temperature of 60 °C further confirmed these trends (Figure S2). Notably, MC 100 samples in time-dependent experiments did not aggregate as extensively as in temperature-dependent experiments, indicating that this behavior is only triggered at higher temperatures (>65 °C) upon more extensive thermal unfolding.

To corroborate the DLS data, CD spectroscopy measurements were conducted to monitor temperature-induced unfolding of each BSA sample with respect to the loss of α-helical secondary structure at higher temperatures. At 25 °C, all BSA samples had similar degrees of α-helicity with an average of ∼62%, and the percentage value decreased with increasing temperature due to thermally induced protein

https://dx.doi.org/10.1021/acs.langmuir.0c02048
Langmuir 2020, 36, 10606−10614

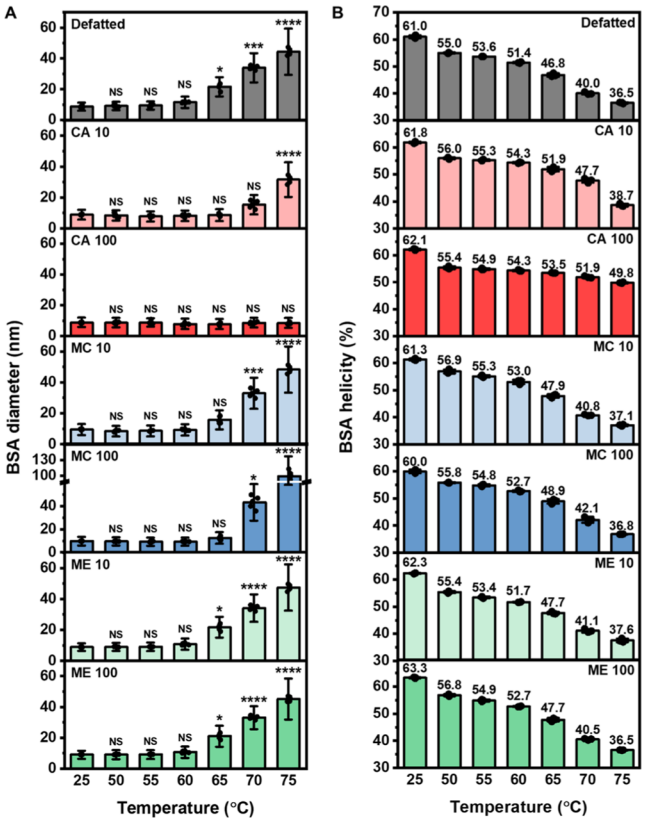

Figure 3. Temperature-dependent DLS and CD spectroscopy measurements to evaluate solution-phase conformational stability of amphiphile-doped BSA proteins. (A) Hydrodynamic diameter of BSA proteins alone and in the presence of CA, MC, and ME at amphiphile/BSA molar ratios of 10:1 and 100:1 as a function of temperature. Data are presented as mean ± standard deviation (sd), where sd is defined as the full width at half-maximum (FWHM)/2.355 [n = 5 technical replicates, one-way analysis of variance (ANOVA) with Dunnett's multiple comparisons test (versus data at 25 °C)]. Dots represent individual data points. (B) Degree of α-helical secondary structure, expressed in percentage values, for BSA alone and in the presence of CA, MC, and ME at amphiphile/BSA molar ratios of 10:1 and 100:1 as a function of temperature obtained from CD spectroscopy experiments. Data were computed from molar residue ellipticity values and are reported as mean ± sd (n = 3). Dots represent individual data points. Mean values are presented on top of each column.

unfolding (Figures 3B and S3).[13,45] While reversible protein unfolding occurs with relatively small temperature increases, irreversible protein unfolding occurs above the onset temperature of aggregation in the range of 60 °C or higher depending on the sample conditions. Thus, we focused on comparing the degree of α-helicity at 65 °C to scrutinize differences in conformational stabilities between the various amphiphile-doped BSA samples. At 65 °C, defatted BSA had the lowest degree of α-helicity with a percentage value around 46.8%, followed by the ME samples with ∼47.7%, and then MC 10 and MC 100 with around 47.9 and 48.9%, respectively. On the other hand, the CA 10 and CA 100 samples maintained a higher degree of α-helicity, with percentage values around 51.9 and 53.5%, respectively. This trend agrees with the DLS data and supports that CA is most effective at increasing BSA conformational stability, followed by MC and then ME.

Upon further increasing the temperature to 70 °C, the CA 10 and CA 100 samples had α-helical values of 47.7 and 51.9%, respectively, while the degree of α-helicity for MC 100 had decreased to 42.1% and all other BSA samples had values around ∼41%. Likewise, at 75 °C, the CA 100 sample had 49.8% α-helicity, while all other samples had similar degrees of α-helicity around ∼37%. Together with the DLS data, these results support that MC 100 has greater conformational stability but lower colloidal stability than defatted BSA, as indicated by its higher onset temperature of aggregation and formation of larger protein aggregates upon sufficiently extensive thermal unfolding.

Additional ionic-strength-dependent DLS experiments further indicated that the amphiphile headgroup−BSA protein interactions were dominated by polar interactions such as hydrogen bonding rather than electrostatic forces (see the Supporting Information and Figure S4). Collectively, the DLS and CD spectroscopy measurements both showed that the stabilizing effectiveness of the amphiphiles was in the order of CA > MC > ME and that the extent of amphiphile-induced protein stability in the solution phase was greater at higher bulk amphiphile concentrations in general.

Real-Time Adsorption Behavior. Next, we investigated the effect of CA, MC, and ME on BSA protein adsorption onto a hydrophilic silica surface by conducting quartz crystal microbalance-dissipation (QCM-D) experiments. The isoelectric point (IEP) of silica is around 3.9,[46] while the IEP of BSA protein is around 5.1.[47] As such, in the pH 7.5 buffer solution, both the silica surface and BSA protein surface are expected to have net negative charges and hence possibly some degree of electrostatic repulsion between them. Nevertheless, BSA proteins can still adsorb onto the silica surface because positively charged regions on the BSA molecular surface can contact the silica surface, yielding attractive electrostatic interactions while hydrogen-bonding and van der Waals interactions can also influence BSA adsorption.[48] The amount and charge of bound amphiphiles are also expected to influence the extent of protein adsorption.

Experimentally, the QCM-D frequency (ΔF) and energy dissipation (ΔD) shifts correspond to the hydrodynamically coupled mass and viscoelastic properties of adsorbed BSA protein molecules, respectively,[33,49,50] and were recorded as a function of time. The time-resolved ΔF shift data indicated monotonic adsorption of BSA proteins in all cases, and most adsorbed proteins remained irreversibly attached, as indicated by a subsequent buffer washing step without protein (Figure 4A). The ΔF shift at adsorption saturation (denoted as $|\Delta F_{max}|$) was analyzed for the different BSA samples, and a larger $|\Delta F_{max}|$ indicates greater adsorption uptake (Figure 4B).

The adsorption of defatted BSA proteins yielded an average $|\Delta F_{max}|$ value of 45.5 Hz, while CA 10 and CA 100 samples tended to have smaller average $|\Delta F_{max}|$ values of 44.1 and 39.9 Hz, respectively. By contrast, MC 10 and MC 100 had average $|\Delta F_{max}|$ values around 45.5 and 47.1 Hz, respectively, whereas the ME 10 and ME 100 samples had average $|\Delta F_{max}|$ values of 44.3 and 44.2 Hz, respectively. Together, these data support that increasing amounts of CA doping tended to decrease BSA adsorption uptake, while MC and ME doping had nearly negligible effects.

The time-resolved ΔD shift mirrored the kinetic profiles observed in the ΔF shift data, and we further analyzed the $|\Delta F_{max}/\Delta D_{max}|$ ratio, whereby a larger ratio indicates a more tightly coupled BSA adlayer and vice versa (Figure 4C,D). Accordingly, it was observed that defatted BSA had an average $|\Delta F_{max}/\Delta D_{max}|$ value of 12.2 Hz × 10^6, while CA 10 and CA

https://dx.doi.org/10.1021/acs.langmuir.0c02048
Langmuir 2020, 36, 10606−10614

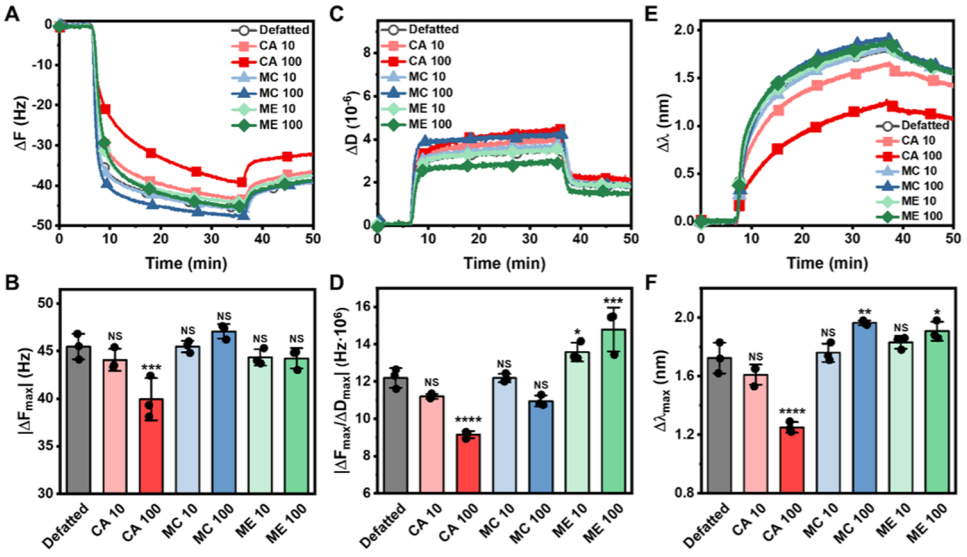

Figure 4. QCM-D and LSPR measurements for tracking real-time adsorption of amphiphile-doped BSA proteins onto silica surfaces. (A) QCM-D frequency (ΔF) shifts as a function of time and (B) the corresponding $|\Delta F_{max}|$ shifts at adsorption saturation. (C) QCM-D energy dissipation (ΔD) shifts as a function of time. (D) $|\Delta F_{max}/\Delta D_{max}|$ values obtained from the data in (A) and (C) at adsorption saturation. (E) LSPR wavelength ($\Delta\lambda$) shifts as a function of time and (F) the corresponding $\Delta\lambda_{max}$ shifts at adsorption saturation. Data in (B), (D), and (F) are presented as mean ± sd [n = 3 biological replicates, one-way ANOVA with Dunnett's multiple comparisons test (versus defatted BSA)]. Dots represent individual data points.

100 samples had smaller average $|\Delta F_{max}/\Delta D_{max}|$ values around 11.2 and 9.1 Hz × 10^6, respectively. On the other hand, MC 10 and MC 100 samples had average $|\Delta F_{max}/\Delta D_{max}|$ values of 12.2 and 10.9 Hz × 10^6, respectively, and ME 10 and ME 100 samples had average $|\Delta F_{max}/\Delta D_{max}|$ values of 13.6 and 14.8 Hz × 10^6, respectively. Together, these results show that CA addition tended to reduce BSA adsorption uptake. Notably, the CA 100 sample had the lowest adsorption uptake and formed the least rigid protein adlayer, which support that high levels of CA doping endow the BSA proteins with greater conformational stability. By contrast, the defatted BSA and MC 10 samples had similar levels of adsorption uptake and adlayer rigidity, while the MC 100 sample tended to result in greater adsorption uptake and less adlayer rigidity. In addition, the ME 10 and ME 100 samples had similar adsorption properties to the defatted BSA control sample. As such, the overall findings indicate that both the type and amount of amphiphile influence the BSA adlayer properties.

In addition to QCM-D measurements, we also conducted localized surface plasmon resonance (LSPR) sensing experiments as a complementary approach to monitor the adsorption of BSA proteins onto silica-coated gold nanodisk arrays. While QCM-D measurements are sensitive to the mass of adsorbed protein molecules and hydrodynamically coupled solvent molecules, i.e., "wet mass", LSPR measurements are sensitive only to the "dry mass" corresponding to adsorbed protein molecules.[51] Furthermore, the LSPR measurement approach has a shorter penetration depth of ~20 nm or less compared to 100−300 nm for the QCM-D technique.[51] Hence, protein adsorption events would occur within a larger fraction of the LSPR-tracked probing volume, which can potentially yield higher surface sensitivity to subtle variations in adsorption behavior and adsorption-related conformational properties. As presented in Figure 4E, BSA protein adsorption was monitored in real time by tracking wavelength shifts ($\Delta\lambda$) of the LSPR extinction peak position, which arise due to the adsorption and spreading of BSA proteins on the sensor surface.[45] Larger $\Delta\lambda$ shifts correspond to greater adsorption uptake, and monotonic $\Delta\lambda$ shift increases were observed in all cases. Most attached BSA molecules were irreversibly adsorbed, as indicated by a buffer washing step.

To compare the different BSA samples, the $\Delta\lambda$ shifts corresponding to adsorption at saturation ($\Delta\lambda_{max}$) were recorded (Figure 4F). For defatted BSA, the average $\Delta\lambda_{max}$ shift was around 1.72 nm, while the CA 10 and CA 100 samples had average $\Delta\lambda_{max}$ shifts around 1.61 and 1.25 nm, respectively. On the other hand, the MC 10 and MC 100 samples had average $\Delta\lambda_{max}$ shifts around 1.76 and 1.96 nm, respectively, while the ME 10 and ME 100 samples had average $\Delta\lambda_{max}$ shifts around 1.83 and 1.91 nm, respectively. Collectively, the results agree well with the trends observed in the QCM-D measurements, while the LSPR measurement signal proved more sensitive to distinguish between the adsorption profiles of different BSA samples. Overall, the data indicate that CA addition reduced BSA adsorption uptake, MC addition increased adsorption uptake when added at high concentrations, and ME addition tended to only slightly increase adsorption uptake. Furthermore, taking into account that there is negligible binding between the ME amphiphile and BSA protein, the slight increase in adsorption uptake for ME-doped BSA samples in the QCM-D and LSPR experiments suggests that free ME can adsorb onto the silica surface.[52]

Adsorption-Related Protein Conformational Changes. To further analyze the adsorption behavior of the different BSA samples, we evaluated the extent of adsorption-related protein conformational changes by calculating the maximum rate of change in the LSPR $\Delta\lambda$ shift during the initial stage of adsorption $(d\Delta\lambda/dt)_{max}$ (Figures 5A and S5).[45,51,53] A larger $(d\Delta\lambda/dt)_{max}$ value indicates more extensive adsorption-related conformational changes, especially protein spreading, whereby the adsorbed protein mass is closer, on average, to the sensor surface. The average $(d\Delta\lambda/dt)_{max}$ value for defatted BSA samples was around 0.74 nm/min, while the

https://dx.doi.org/10.1021/acs.langmuir.0c02048
Langmuir 2020, 36, 10606−10614

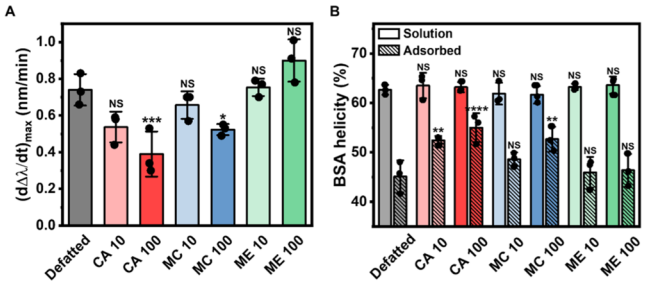

Figure 5. Evaluation of adsorption-related protein conformational changes for amphiphile-doped BSA proteins. (A) Maximum rate of change in the $\Delta\lambda$ shift during the initial stage of adsorption $(d\Delta\lambda/dt)_{max}$. (B) Fractional percentage of α-helical secondary structure for BSA proteins in solution and in the adsorbed state, as measured by ATR-FTIR spectroscopy experiments. Data in (A) and (B) are presented as mean ± sd [n = 3 biological replicates, one-way ANOVA with Dunnett's multiple comparisons test (versus defatted BSA) in (A) and two-way ANOVA with Dunnett's multiple comparisons test for all samples in solution (versus defatted BSA in solution) and separately for all samples in the adsorbed state (versus defatted BSA in the adsorbed state) in (B)]. Dots represent individual data points.

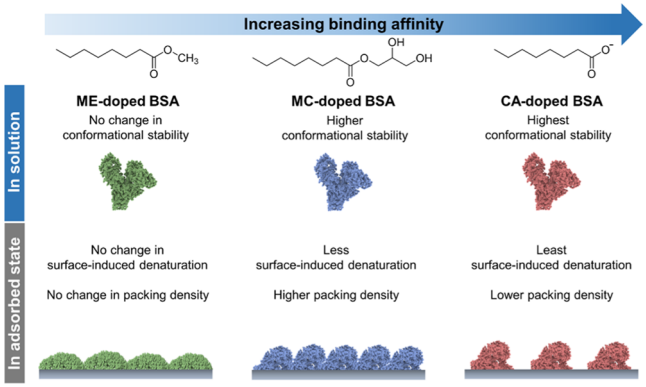

Figure 6. Schematic illustration summarizing how the CA, MC, and ME amphiphiles affect the solution-phase conformational stability and adsorption properties of BSA proteins. ME had low binding affinity to BSA proteins and hence largely negligible effects. MC moderately enhanced conformational stability, which reduced adsorption-related denaturation, while the nonionic character of MC allowed MC-doped BSA protein adlayers to have relatively higher packing densities. Likewise, CA strongly enhanced conformational stability, which also reduced adsorption-related denaturation. However, the anionic character of CA created more repulsive interactions between CA-doped BSA proteins, which led to CA-doped BSA protein adlayers with relatively lower packing densities.

CA 10 and CA 100 samples had average $(d\Delta\lambda/dt)_{max}$ values of 0.54 and 0.39 nm/min, respectively. Likewise, the MC 10 and MC 100 samples had average $(d\Delta\lambda/dt)_{max}$ values of 0.66 and 0.52 nm/min, respectively, whereas the ME 10 and ME 100 samples had average $(d\Delta\lambda/dt)_{max}$ values around 0.75 and 0.90 nm/min, respectively. The findings indicate that both CA and MC doping reduced the extent of adsorption-related BSA conformational changes. In this respect, CA was more effective than MC in maintaining protein conformational stability. On the other hand, the ME 10 and ME 100 samples underwent protein spreading in the adsorbed state to similar extents to the defatted BSA control.

Attenuated total reflection-Fourier transform infrared (ATR-FTIR) spectroscopy experiments were also performed to quantitatively determine the fractional percentage of α-helical secondary structure for the BSA protein samples in solution and in the adsorbed state (Figures 5B and S6). In solution, all BSA samples had similar degrees of α-helicity, with values around ~62.8%. By contrast, in the adsorbed state, defatted BSA samples underwent partial unfolding and the percentage of α-helical character decreased to around 45.1%. In marked contrast, the CA 10, CA 100, MC 10, and MC 100 samples maintained α-helical character to a greater extent, and the corresponding values in the adsorbed state were 52.4, 55.0, 48.6, and 52.7%. This trend agrees well with the LSPR measurement data and provides additional evidence that both CA and MC stabilize BSA to reduce the extent of adsorption-related protein conformational changes. Furthermore, the ATR-FTIR spectroscopy results also show that CA confers greater conformational stability on BSA proteins than MC. On the other hand, adsorption of the ME 10 and ME 100 samples caused similar losses in α-helicity that mirrored the defatted BSA case, with average α-helicity values of 46.0 and 46.4%, respectively, in the adsorbed state. As such, the data indicate that ME doping does not endow BSA proteins with greater conformational stability.

Schematic Overview of Amphiphile Effects. Figure 6 presents a schematic illustration that summarizes the main experimental findings and describes how CA, MC, and ME amphiphiles affect BSA protein adsorption behavior on a case-by-case basis. We begin our discussion with the ME case because ME had the least effect on BSA adsorption, which is consistent with the fluorescence spectroscopy data that indicated a weak binding interaction between BSA and ME. As such, ME-doped BSA samples had similar solution-phase conformational stability and adsorption behavior to the defatted BSA control sample. On the other hand, CA had the highest binding affinity to BSA, and CA-doped BSA samples exhibited the greatest solution-phase conformational stability. Moreover, while less surface-induced denaturation typically leads to greater total adsorption uptake due to a smaller contact area per molecule, CA-doped BSA proteins also had the lowest total adsorption uptake and consequently lowest packing density of adsorbed protein molecules.[32] This trend occurred because the carboxylic acid functional groups of CA are negatively charged and thus CA-doped BSA proteins have intermolecular repulsion, which limits the surface coverage of adsorbed protein molecules.

Between these two cases, we also observed interesting results with the MC amphiphile, whereby it moderately enhanced solution-phase protein conformational stability and led to the formation of well-packed protein adlayers. MC is nonionic, so there was appreciably less intermolecular repulsion between MC-doped BSA proteins, which enabled higher total adsorption uptake due to greater packing density within the BSA adlayer. While CA had notable effects even at a 10:1 CA/BSA molar ratio, the effects of MC on BSA adsorption properties were most clearly observed at a 100:1 MC/BSA molar ratio because MC has lower binding affinity to BSA than CA. Together, these data support that amphiphile doping can affect BSA adsorption properties by two main effects, including enhancing conformational stability and modulating protein−protein interactions in the adsorbed state. Rational selection of the amphiphile type and amount used to stabilize BSA proteins can therefore enable control over BSA adlayer properties in terms of adsorption-related denaturation and packing density.

https://dx.doi.org/10.1021/acs.langmuir.0c02048
Langmuir 2020, 36, 10606−10614

CONCLUSIONS

In this study, we have employed a wide range of biophysical and surface-sensitive measurement techniques to characterize the effects of CA, MC, and ME amphiphiles on BSA conformational stability and adsorption behavior on silica surfaces. While each amphiphile had an 8-carbon-long, saturated hydrocarbon chain, we observed marked differences in the binding affinity of each amphiphile to BSA proteins, which indicates that the amphiphile headgroup also plays an important role in binding interactions. Both CA and MC demonstrated binding to BSA proteins and improved solution-phase conformational stability along with reducing surface-induced denaturation in the adsorbed state. Due to difference in binding affinity, CA was generally effective at both 10:1 and 100:1 amphiphile/BSA molar ratios, while MC was more effective at the 100:1 molar ratio. Notably, the anionic character of CA fatty acids led to reduced packing densities within CA-doped BSA protein adlayers, whereas the nonionic character of MC monoglycerides enabled higher packing densities within MC-doped BSA protein adlayers. These findings also agree well with the temperature-dependent protein aggregation data, indicating that CA modulates both conformational and colloidal stabilities, whereas MC mainly influences conformational stability. While CA is typically used to dope BSA proteins as part of purification processes, our findings point to the potential significance of doping BSA proteins with MC to create purified BSA proteins with improved properties for BSA adlayer-based surface passivation applications.

ASSOCIATED CONTENT

Supporting Information

The Supporting Information is available free of charge at https://pubs.acs.org/doi/10.1021/acs.langmuir.0c02048.

CD and ATR-FTIR spectroscopy methods, fluorescence spectroscopy data (Table S1), DLS data (Figures S1 and S2), CD data (Figure S3), ionic-strength-dependent DLS data (Figure S4), LSPR data (Figure S5), and ATR-FTIR spectroscopy data (Figure S6), and the determination of static quenching and on amphiphile headgroup−BSA interactions (PDF)

AUTHOR INFORMATION

Corresponding Authors

Joshua A. Jackman − *School of Chemical Engineering, Sungkyunkwan University, Suwon 16419, Republic of Korea;* orcid.org/0000-0002-1800-8102; Email: jjackman@skku.edu

Nam-Joon Cho − *School of Materials Science and Engineering, Nanyang Technological University, Singapore 639798;* orcid.org/0000-0002-8692-8955; Email: njcho@ntu.edu.sg

Authors

Gamaliel Junren Ma − *School of Materials Science and Engineering, Nanyang Technological University, Singapore 639798;* orcid.org/0000-0002-6740-1031

Abdul Rahim Ferhan − *School of Materials Science and Engineering, Nanyang Technological University, Singapore 639798;* orcid.org/0000-0003-3238-3125

Complete contact information is available at: https://pubs.acs.org/10.1021/acs.langmuir.0c02048

Notes

The authors declare no competing financial interest.

ACKNOWLEDGMENTS

This work was supported by the National Research Foundation of Singapore through a Competitive Research Programme grant (NRF-CRP10-2012-07) and a Proof-of-Concept grant (NRF2015NRF-POC0001-19) and by the National Research Foundation of Korea (NRF) grant funded by the Korean government (MSIT) (no. 2020R1C1C1004385).

REFERENCES

(1) Gray, J. J. The interaction of proteins with solid surfaces. *Curr. Opin. Struct. Biol.* **2004**, *14*, 110−115.

(2) Meyers, S. R.; Grinstaff, M. W. Biocompatible and bioactive surface modifications for prolonged in vivo efficacy. *Chem. Rev.* **2011**, *112*, 1615−1632.

(3) Bhakta, S. A.; Evans, E.; Benavidez, T. E.; Garcia, C. D. Protein adsorption onto nanomaterials for the development of biosensors and analytical devices: A review. *Anal. Chim. Acta* **2015**, *872*, 7−25.

(4) Pinholt, C.; Hartvig, R. A.; Medlicott, N. J.; Jorgensen, L. The importance of interfaces in protein drug delivery − why is protein adsorption of interest in pharmaceutical formulations? *Expert Opin. Drug Delivery* **2011**, *8*, 949−964.

(5) Schöttler, S.; Becker, G.; Winzen, S.; Steinbach, T.; Mohr, K.; Landfester, K.; Mailänder, V.; Wurm, F. R. Protein adsorption is required for stealth effect of poly (ethylene glycol)-and poly (phosphoester)-coated nanocarriers. *Nat. Nanotechnol.* **2016**, *11*, 372.

(6) Rabe, M.; Verdes, D.; Seeger, S. Understanding protein adsorption phenomena at solid surfaces. *Adv. Colloid Interface Sci.* **2011**, *162*, 87−106.

(7) Tsapikouni, T. S.; Missirlis, Y. F. Protein−material interactions: From micro-to-nano scale. *Mater. Sci. Eng., B* **2008**, *152*, 2−7.

(8) Yano, Y. F. Kinetics of protein unfolding at interfaces. *J. Phys.: Condens. Matter* **2012**, *24*, No. 503101.

(9) Ariga, K.; Ji, Q.; Hill, J. P.; Bando, Y.; Aono, M. Forming nanomaterials as layered functional structures toward materials nanoarchitectonics. *NPG Asia Mater.* **2012**, *4*, No. e17.

(10) Ariga, K.; Ji, Q.; Nakanishi, W.; Hill, J. P.; Aono, M. Nanoarchitectonics: a new materials horizon for nanotechnology. *Mater. Horiz.* **2015**, *2*, 406−413.

(11) Karlsson, M.; Ekeroth, J.; Elwing, H.; Carlsson, U. Reduction of irreversible protein adsorption on solid surfaces by protein engineering for increased stability. *J. Biol. Chem.* **2005**, *280*, 25558−25564.

(12) Park, J. H.; Sut, T. N.; Jackman, J. A.; Ferhan, A. R.; Yoon, B. K.; Cho, N.-J. Controlling adsorption and passivation properties of bovine serum albumin on silica surfaces by ionic strength modulation and cross-linking. *Phys. Chem. Chem. Phys.* **2017**, *19*, 8854−8865.

(13) Park, J. H.; Jackman, J. A.; Ferhan, A. R.; Ma, G. J.; Yoon, B. K.; Cho, N.-J. Temperature-induced denaturation of BSA protein molecules for improved surface passivation coatings. *ACS Appl. Mater. Interfaces* **2018**, *10*, 32047−32057.

(14) Peng, Q.; Zhang, S.; Yang, Q.; Zhang, T.; Wei, X.-Q.; Jiang, L.; Zhang, C.-L.; Chen, Q.-M.; Zhang, Z.-R.; Lin, Y.-F. Preformed albumin corona, a protective coating for nanoparticles based drug delivery system. *Biomaterials* **2013**, *34*, 8521−8530.

(15) del Río, J. S.; Henry, O. Y.; Jolly, P.; Ingber, D. E. An antifouling coating that enables affinity-based electrochemical biosensing in complex biological fluids. *Nat. Nanotechnol.* **2019**, *14*, 1143−1149.

(16) Tan, J. Y. B.; Yoon, B. K.; Ma, G. J.; Sut, T. N.; Cho, N.-J.; Jackman, J. A. Unraveling how ethanol-induced conformational changes affect BSA protein adsorption onto silica surfaces. *Langmuir* **2020**, *36*, 9215.

(17) Ma, G. J.; Ferhan, A. R.; Sut, T. N.; Jackman, J. A.; Cho, N.-J. Understanding how natural sequence variation in serum albumin

proteins affects conformational stability and protein adsorption. *Colloids Surf., B* **2020**, *194*, No. 111194.
(18) Peters, T. Serum Albumin. In *Advances in Protein Chemistry*; Elsevier, 1985; Vol. *37*, pp 161−245.
(19) Kelley, D.; McClements, D. Interactions of bovine serum albumin with ionic surfactants in aqueous solutions. *Food Hydrocolloids* **2003**, *17*, 73−85.
(20) Hamilton, J. A. NMR reveals molecular interactions and dynamics of fatty acid binding to albumin. *Biochim. Biophys. Acta, Gen. Subj.* **2013**, *1830*, 5418−5426.
(21) Wasylewski, Z.; Kozik, A. Protein—non-ionic detergent interaction: interaction of bovine serum albumin with alkyl glucosides studied by equilibrium dialysis and infrared spectroscopy. *Eur. J. Biochem.* **1979**, *95*, 121−126.
(22) Kragh-Hansen, U.; Watanabe, H.; Nakajou, K.; Iwao, Y.; Otagiri, M. Chain length-dependent binding of fatty acid anions to human serum albumin studied by site-directed mutagenesis. *J. Mol. Biol.* **2006**, *363*, 702−712.
(23) Ojha, B.; Das, G. Role of hydrophobic and polar interactions for BSA−amphiphile composites. *Chem. Phys. Lipids* **2011**, *164*, 144−150.
(24) Gelamo, E. L.; Tabak, M. Spectroscopic studies on the interaction of bovine (BSA) and human (HSA) serum albumins with ionic surfactants. *Spectrochim. Acta, Part A* **2000**, *56*, 2255−2271.
(25) Nielsen, A. D.; Borch, K.; Westh, P. Thermochemistry of the specific binding of C12 surfactants to bovine serum albumin. *Biochim. Biophys. Acta, Protein Struct. Mol. Enzymol.* **2000**, *1479*, 321−331.
(26) Chakraborty, T.; Chakraborty, I.; Moulik, S. P.; Ghosh, S. Physicochemical and conformational studies on BSA− surfactant interaction in aqueous medium. *Langmuir* **2009**, *25*, 3062−3074.
(27) Ghosh, S.; Dey, J. Binding of fatty acid amide amphiphiles to bovine serum albumin: role of amide hydrogen bonding. *J. Phys. Chem. B* **2015**, *119*, 7804−7815.
(28) De, S.; Girigoswami, A.; Das, S. Fluorescence probing of albumin−surfactant interaction. *J. Colloid Interface Sci.* **2005**, *285*, 562−573.
(29) Boyer, P. D.; Lum, F. G.; Ballou, G. A.; Luck, J. M.; Rice, R. G. The combination of fatty acids and related compounds with serum albumin I. stabilization against heat denaturation. *J. Biol. Chem.* **1946**, *162*, 181−198.
(30) Boyer, P. D.; Ballou, G. A.; Luck, J. M. The combination of fatty acids and related compounds with serum albumin II. Stabilization against urea and guanidine denaturation. *J. Biol. Chem.* **1946**, *162*, 199−208.
(31) Deep, S.; Ahluwalia, J. C. Interaction of bovine serum albumin with anionic surfactants. *Phys. Chem. Chem. Phys.* **2001**, *3*, 4583−4591.
(32) Ma, G. J.; Ferhan, A. R.; Jackman, J. A.; Cho, N.-J. Conformational flexibility of fatty acid-free bovine serum albumin proteins enables superior antifouling coatings. *Commun. Mater.* **2020**, *1*, No. 45.
(33) Cho, N.-J.; Frank, C. W.; Kasemo, B.; Höök, F. Quartz crystal microbalance with dissipation monitoring of supported lipid bilayers on various substrates. *Nat. Protoc.* **2010**, *5*, 1096.
(34) Jackman, J. A.; Zhdanov, V. P.; Cho, N.-J. Nanoplasmonic biosensing for soft matter adsorption: kinetics of lipid vesicle attachment and shape deformation. *Langmuir* **2014**, *30*, 9494−9503.
(35) Zan, G. H.; Jackman, J. A.; Kim, S. O.; Cho, N. J. Controlling lipid membrane architecture for tunable nanoplasmonic biosensing. *Small* **2014**, *10*, 4828−4832.
(36) Thumser, A. E.; Buckland, A. G.; Wilton, D. C. Monoacylglycerol binding to human serum albumin: evidence that monooleoylglycerol binds at the dansylsarcosine site. *J. Lipid Res.* **1998**, *39*, 1033−1038.
(37) Duff, S. M.; Kalambur, S.; Boyle-Roden, E. Serum albumin binds β-and α-monoolein in vitro. *J. Nutr.* **2001**, *131*, 774−778.
(38) Arvidsson, E. O.; Belfrage, P. Monoglyceride-protein interaction. The binding of monoolein to native human serum albumin. *Acta Chem. Scand.* **1969**, *23*, 232−236.
(39) Spector, A. A.; John, K.; Fletcher, J. E. Binding of long-chain fatty acids to bovine serum albumin. *J. Lipid Res.* **1969**, *10*, 56−67.
(40) Morrisett, J. D.; Pownall, H.; Gotto, A. Bovine serum albumin. Study of the fatty acid and steroid binding sites using spin-labeled lipids. *J. Biol. Chem.* **1975**, *250*, 2487−2494.
(41) Stern, O.; Volmer, M. Über die abklingzeit der fluoreszenz. *Phys. Z* **1919**, *20*, 183−188.
(42) Iovescu, A.; Băran, A.; Stîngă, G.; Cantemir-Leontieş, A. R.; Maxim, M. E.; Anghel, D. F. A combined binding mechanism of nonionic ethoxylated surfactants to bovine serum albumin revealed by fluorescence and circular dichroism. *J. Photochem. Photobiol., B* **2015**, *153*, 198−205.
(43) Min, J.; Meng-Xia, X.; Dong, Z.; Yuan, L.; Xiao-Yu, L.; Xing, C. Spectroscopic studies on the interaction of cinnamic acid and its hydroxyl derivatives with human serum albumin. *J. Mol. Struct.* **2004**, *692*, 71−80.
(44) Zhu, T.-T.; Zhang, Y.; Luo, X.-A.; Wang, S.-Z.; Jia, M.-Q.; Chen, Z.-X. Difference in binding of long-and medium-chain fatty acids with serum albumin: The role of macromolecular crowding effect. *J. Agric. Food Chem.* **2018**, *66*, 1242−1250.
(45) Jackman, J. A.; Ferhan, A. R.; Yoon, B. K.; Park, J. H.; Zhdanov, V. P.; Cho, N.-J. Indirect nanoplasmonic sensing platform for monitoring temperature-dependent protein adsorption. *Anal. Chem.* **2017**, *89*, 12976−12983.
(46) Cuddy, M. F.; Poda, A. R.; Brantley, L. N. Determination of isoelectric points and the role of pH for common quartz crystal microbalance sensors. *ACS Appl. Mater. Interfaces* **2013**, *5*, 3514−3518.
(47) Jachimska, B.; Pajor, A. Physico-chemical characterization of bovine serum albumin in solution and as deposited on surfaces. *Bioelectrochemistry* **2012**, *87*, 138−146.
(48) Kubiak-Ossowska, K.; Tokarczyk, K.; Jachimska, B.; Mulheran, P. A. Bovine serum albumin adsorption at a silica surface explored by simulation and experiment. *J. Phys. Chem. B* **2017**, *121*, 3975−3986.
(49) Peeters, M.; Jiménez-Monroy, K.; Libert, C.; Eurlings, Y.; Cuypers, W.; Wackers, G.; Duchateau, S.; Robaeys, P.; Nesládek, M.; Van Grinsven, B.; et al. Real-time monitoring of aptamer functionalization and detection of Ara H1 by electrochemical impedance spectroscopy and dissipation-mode quartz crystal microbalance. *J. Biosens. Bioelectron.* **2014**, *5* (3), 1000155.
(50) Neupane, S.; De Smet, Y.; Renner, F. U.; Losada-Pérez, P. Quartz crystal microbalance with dissipation monitoring: A versatile tool to monitor phase transitions in biomimetic membranes. *Front. Mater.* **2018**, *5*, 46.
(51) Jackman, J. A.; Ferhan, A. R.; Cho, N.-J. Nanoplasmonic sensors for biointerfacial science. *Chem. Soc. Rev.* **2017**, *46*, 3615−3660.
(52) Slawson, V.; Mead, J. F. Stability of unsaturated methyl esters of fatty acids on surfaces. *J. Lipid Res.* **1972**, *13*, 143−146.
(53) Ferhan, A. R.; Jackman, J. A.; Sut, T. N.; Cho, N.-J. Quantitative comparison of protein adsorption and conformational changes on dielectric-coated nanoplasmonic sensing arrays. *Sensors* **2018**, *18*, 1283.

https://dx.doi.org/10.1021/acs.langmuir.0c02048
Langmuir 2020, 36, 10606−10614